The impact of spin up and resolution on the representation of a clear convective boundary layer over London in order 100m grid-length versions of the Met Office Unified Model

Article

Accepted Version

The impact of spin up and resolution on the representation of a clear convective boundary layer over London in order 100m grid-length versions of the Met Office Unified Model.

H.W.Lean[1], J.F.Barlow[2], C.H.Halios[2]

1. MetOffice@Reading, Meteorology Building, University of Reading, Reading RG6 6BB
2. Department of Meteorology, University of Reading, Reading RG6 6BB

*Corresponding author: *Humphrey.lean@metoffice.gov.uk*

Key words: Convective boundary layer, turbulence, mixing height, urban meteorology, turbulence grey zone, spin up effects, spectral analysis, Doppler lidar.

Abstract

With a number of operational centres looking forward to the possibilities of "city scale" NWP and climate modelling it is important to understand the behaviour of order 100m models over cities. A key issue is how to handle the representation of partially resolved turbulence in these models. In this paper we compare the representation of a clear convective boundary layer case in London in 100m and 50m grid-length versions of the Unified Model (MetUM) with observations. Comparison of Doppler lidar observations of the vertical velocity shows that convective overturning in the boundary layer is broadly well represented in terms of its depth and magnitude. The role of model resolution was investigated by comparing a 50m grid-length model with the 100m one. It is found that, although going to 50m grid-length does not greatly change many of the bulk properties (mixing height, heat flux profiles, etc.) the spatial structure of the overturning is significantly different. This is confirmed with spectral analysis which shows that the 50m model resolves significantly more of the energetic eddies, and a length scale analysis that shows the 50m and 100m models produce convective structures 2-3 times larger than observed. We conclude that, for the MetUM, model grid-lengths of order 100m may well be sufficient for predicting many bulk and statistical properties of convective boundary layers however the details of the spatial structures around convective overturning in these situations are likely to be still under-resolved. Spin up artefacts emanating from the inflow boundary of the model are investigated by comparing with a smaller 100m grid-length domain which is more dominated by such effects. These manifest themselves as along wind boundary layer rolls which produce a less realistic comparison with the lidar observations. A stability analysis is presented in order to better understand the formation of these rolls.

1. Introduction

Operational regional NWP has been transformed in the last ten years by the introduction of km scale "convection permitting models" (Clark et al., 2016). More recently these models have been used for climate simulations (Kendon et al., 2014). These models have proved particularly useful because of their improved representation of convection (Prein et al., 2015, Clark et al., 2016). Higher resolution has meant that larger cities and their impact on the atmosphere can now be at least crudely represented within NWP and climate models (e.g. Holt and Pullen, 2007, Miao et al., 2009, Bohnenstengel et al., 2011, Chen et al., 2011) although smaller cities and neighbourhood scale features within larger ones cannot. With the continuing advances in available computer power a number of operational centres are now carrying out research into a new generation of city scale models at turbulence permitting (O(100m)) scales (Leroyer et al., 2014, Ronda et al., 2017). The motivation for this is to improve small scale forecasts of hazards (urban heat, flooding, poor air quality) on both weather and climate timescales. In contrast to the current generation of km scale models these models would provide the potential to represent features on neighbourhood scales (e.g. parks, rivers etc) and their effect on the local meteorology.

There are two aspects to the problem of developing urban models at these scales. Firstly there is the problem of the best way to represent the urban surface (Best et al., 2015). Barlow et al. (2017) identified the main problems as being heterogeneity on many scales, and anthropogenic effects. Models at 100m scales will have to operate between the traditional convection permitting NWP regime where there are many buildings per grid-box and the very high resolution regime of LES modelling of individual buildings and streets (the so called "building grey zone"). There is also the need to treat the vertical extent of buildings in high rise cities and small groups of tall buildings. It will also be very important to introduce

realistic anthropogenic fluxes of heat and moisture. This can either be done through interfacing the model to datasets of anthropogenic emissions (Allen et al., 2011) or by incorporating parameterisations of building and transport emissions (e.g. Bohnenstengel et al., 2014).

The second part of the problem is the behaviour of the atmospheric model itself in the turbulence permitting regime. O(100m) grid-length models will operate in the boundary layer "grey zone" or "terra incognita" (Wyngaard, 2004, Honnert et al., 2011). There has been a good deal of work within the Met Office on pushing the Unified Model (MetUM) to sub kilometre scales. A 100m grid-length MetUM configuration was used to simulate cold pools in valleys which would have been too small to resolve with the operational 1.5km model (Vosper et al., 2013) giving good agreement with observations. Models with several grid-lengths between 1km and 100m were compared to aircraft observations of stratocumulus (Boutle et al., 2014). Hanley et al., 2016) investigated explicit representation of tornadoes on the US Great Plains with a 100m model. Similar UM configurations were also used to investigate the resolution dependence of the representation of deep convection over the UK as part of the DYMECS project (Stein et al., 2015, Hanley et al., 2015). Elsewhere in the community there have been a number of experiments with sub-km NWP models of cities (Ronda et al., 2017, Leroyer et al., 2014).

This paper addresses this second part of the problem in the case of clear convective boundary layers. In the current work, the model is run with the same urban surface scheme (Best, 2005) as the 1.5km operational model used at the time of the case being studied. Even though the representation of the urban surface will be imperfect, we would still expect benefits from resolving relatively short range variations in the surface properties – in particular the surface type and orography. The former allows study of changes of boundary layer properties as air flows over the city. This approach has been highlighted by Ronda et al. (2017) who used

detailed surface input data in a 100m grid-length WRF configuration to produce neighbourhood scale forecasts during a summer period in Amsterdam.

Of particular relevance to this paper is the DYMECS work mentioned above which concluded that MetUM configurations with grid-lengths smaller than 1km do better for deep convection than the operational 1.5km model, (better convection lifecycle, distribution of rainrates, cell sizes etc) but there are still issues. In particular, if the model is run with a 3D Smagorinsky (Smagorinsky, 1963) subgrid mixing scheme with the usual LES value of mixing length of 0.2 of the grid-length, convective updrafts and cells tend to become too narrow at the highest resolutions (Stein et al., 2014, Nicol et al., 2015). This is thought to be due to the scheme not correctly representing the partially resolved turbulence. The role of the subgrid mixing scheme is to represent the turbulence which is not resolved but this balance is, overall, not producing enough turbulence. The behaviour is therefore sensitive to the subgrid mixing scheme used and so the development of suitable schemes is of prime importance.

There has also been similar work to investigate the behaviour of partially resolved turbulence in convective boundary layers – in particular the transition from high resolution LES simulations to lower resolution mesoscale simulations (Efstathiou et al., 2015). Efstathiou et al., 2016) compared the representation of morning boundary layer development in 50m LES with two grey zone boundary layer implementations at lower resolutions (down to 3200m). They evaluated the resulting deficiencies in either evolution of TKE or the amount of instability in the profiles and concluded that both formulations have strengths and weaknesses which highlights the inevitable issues with resolutions that are currently computationally feasible. Ching et al., (2014) investigated the generation of convectively induced secondary circulations in models of various gridlengths and showed that these are incompatible with parameterised boundary layer schemes. Miao et al., (2008) looked at the boundary layer structure over Beijing in a 500m grid-length WRF model with particular emphasis on the

formation of Horizontal Convective Rolls (HCRs) over the urban area. Of relevance to the current paper they concluded that HCRs are more likely over urban areas due to shear produced by the rough surface.

This work uses observations of turbulence in a dry, cloudless convective boundary layer case in London to understand the impact of resolution and domain size on simulated urban convective overturning in 100m and 50m gridlength models running in LES mode. These aspects were chosen for detailed study due to their practical importance for future city scale models. This paper assesses how physically realistic the convective structures appear to be by comparison with observations and theory. Spectral analysis is used to understand the effects of varying the model resolution.Conclusions are drawn about spin up effects at model boundaries and the development of the convective urban boundary layer as it grows across the city.

2. Model, observational and case details.

2.1 Models

The MetUM, version 5.2 onwards, solves non-hydrostatic, deep-atmosphere dynamics using a semi-implicit, semi-Lagrangian numerical scheme (Davies et al., 2005). The model includes a comprehensive set of parameterisations, including boundary layer (Lock et al., 2000) and mixed-phase cloud microphysics (Wilson et al., 1999). Although the model contains an option for convection parameterisation this is switched off in the configurations described here. Of importance to the work described here is the surface scheme which is JULES (Best, M et al., 2011). As part of this surface scheme the models used in the current work incorporated a one tile urban scheme described by Best (2005). This scheme sometimes results in a lag in warming up of urban surfaces in the morning (King and Bohenstengel pers. comm. 2015, Finnenkoeter pers. comm. 2018) but was used here because it was the scheme

121 in operational use at the time of this work. The model runs on a rotated latitude/longitude
122 horizontal grid with Arakawa C staggering and a terrain-following hybrid-height vertical
123 coordinate with Charney-Philips staggering. The standard level set as used in the UKV model
124 has 70 levels in the vertical up to the model top at 40 km. In order to increase the resolution
125 in the boundary layer, the distribution of the levels near the ground is quadratic so, for
126 example, there are 16 levels in the lowest 1km of the atmosphere.

127 For the research reported in this paper a nested set of model configurations were run with
128 MetUM version 8.1 as detailed in Figure 1 and table 1. A 500m grid-length model covering
129 southern and central England was one way nested within the UKV model. The UKV is a
130 1.5km grid-length UK model used for operational forecasting. The "V" in the name UKV
131 refers to the fact that a variable resolution grid is used with lower resolution around the
132 outside. As discussed by (Tang et al., 2013) the variable resolution enables a larger domain to
133 be used a lower cost to avoid boundary spin up effects in the area of interest. Nested in the
134 500m model was a 100m model centred on London with an 80kmx80km domain henceforth
135 referred to as U100. This was the largest domain that it was thought practical to run due to
136 computational constraints. In order to further understand the effects of resolution a 50m
137 model, U50, was also run over the same area as U100 and also nested in the 500m model. In
138 order to investigate spin up effects at model boundaries, we also present some results from a
139 100m model with the same configuration and also centred on the same point in central
140 London but running on a smaller 30 km x 30 km domain, referred to as U100S. Although
141 1.5km and 500m models were run as part of the set of nested models, results from them are
142 not reported since they are too coarse grid-length to explicitly represent the convective
143 overturning which is the subject of this paper.

144 The model configurations were the same as that used for work on convection at similar
145 resolutions (Hanley et al., 2015) and are summarised in Table 1. Apart from grid-length

dependent changes such as timestep and solver tolerance the main difference with resolution was a switch over from using 2D Smagorinsky mixing with the vertical mixing being carried out by the boundary layer scheme in the UKV to using 3D Smagorinsky (c_s=0.2) in the 500m,100m and 50m grid-length configurations. Is should be noted that more recent UM configurations a scale aware blending scheme is used which blends between the boundary layer scheme and 3D Smagorinsky according to the ratio of boundary layer height and grid-length (Boutle et al., 2014). This was not used here because it was thought that using 3D Smagorinsky would be a cleaner test of the model in LES mode. In addition, in convective boundary layer situations such as investigated here, one would expect the blended scheme to operate in the 3D Smagorinsky limit in order 100m grid-length models. The 500m,100m and 50m grid-length configurations used a 140 level set in the vertical which consisted of the standard 70 level set doubled all the way up. The orography and land use data were based on 100m and 25m datasets respectively and became more detailed in the 500m, 100m and 50m grid-length models commensurate with the resolution. The land use dataset used was the ITE dataset (Bunce et al 1990). The urban fraction in the land use data in U100 is shown in Figure 1 – at this scale many neighbourhood scale features of the city including parks and the river can clearly be seen.

2.2 Observations.

The observations used here were obtained from the ACTUAL project (Lane et al., 2013, Barlow et al., 2015, Halios and Barlow, 2018) measurement sites in London: the BT Tower (lat. 51^0 31' 17,6'' W lon. 0^0 08' 20.36'' N) and the Westminster City Council (WCC) roof-top site (lat. 51^0 31' 16.31'' N lon. 0^0 09' 38.33'' W). The BT Tower is the tallest building within several kilometres, with good exposure to winds in all directions. Within 10 km of the BT Tower the land surface cover is a mixture of residential and commercial with a mean building height of 8.8 ± 3 m, roughness length within central London is estimated to be 0.87

± 0.48 m, and the displacement height 4.3 ± 1.9 m (Wood et al., 2010). There are two large parks nearby: Regent's Park (1.66 km^2) approximately 0.64 km north-west of the Tower; Hyde Park (2.53 km^2) approx. 1.7 km to the south-west. It should be noted that the source area for the BT Tower is approximately 2-3 km in scale in convective conditions, 10-20 km in neutral (Helfter et al., 2011), and represents a mixture of urban and vegetative surfaces.

Two identical instrumentation platforms were used for turbulent flux measurements as fully described in Barlow et al. (2015). In this paper, only data from the sonic anemometer on top of the BT Tower were used (Gill Instruments R3-50). The head of the sonic anemometer was placed at 190 m a.g.l. on the BT Tower, the instrument being clamped to a pole on the top of an open lattice scaffolding tower of 12.3 m height on top of the main structure, meaning that the sensor head was 0.76 m higher than the lattice. A full description of the lattice is given in Barlow et al. (2011), where it was deduced from wind tunnel tests that there is only slight flow distortion at the height of the sensor due to the lattice. The sonic anemometer was sampled at 20 Hz.

A heterodyne Doppler lidar (Halo-Photonics "Streamline") with scanning capability was installed on the roof-top of the WCC site to measure the vertical structure of the urban boundary layer. The instrument operated at 1.5 μm wavelength; the pulse repetition frequency was 20 kHz, with integrated signals being output every 3.6 s; the sampling frequency was 30 MHz, and the return signal was resolved into 30 m long range gates. Within the first three gates of the lidar (90m), returns were of insufficient quality; therefore results are presented from the fourth gate upwards, mid-gate height being 124 m a.g.l. once the height of the WCC building at the location of the lidar is taken into account.

Two modes of operation were used: a) continuous stare mode (pointing vertically) and b) Doppler Beam Swinging (DBS) mode for measuring the vertical wind profile (Lane et al.

2013). The DBS mode sampled in three orthogonal directions: vertically, tilted 15° off-zenith to east and to north. The DBS scan cycle lasted approximately 21 s, the time interval between the start of scans in DBS mode was 120 s, and the lidar was in vertical stare mode in the intervening 99 s. Hourly-averaged profiles of vertical velocity variance, $\sigma_w{}^2(z)$, were derived from the vertical stares. Due to the limited sampling rate a spectral correction was applied according to Barlow et al. (2015). Whereas boundary layer height is often defined as the height of the capping inversion in convective conditions, the mixing height, z_{MH}, is the depth of the layer adjacent to the ground over which pollutants become dispersed by turbulence (Seibert, 2000). Mixing height was estimated from the corrected variance profiles by applying a simple threshold method: the mixing height was taken as the gate up to which $\sigma_w{}^2(z) > 0.1\text{m}^2\ \text{s}^{-2}$. To account for uncertainty in the choice of threshold, its value was perturbed by 21 steps of up to ± 30%, and the resulting mean was taken as z_{MH}, and maximum and minimum values were taken as the uncertainty bounds (Barlow et al. 2015).

To estimate the spectral energy density for the lidar a spectral splicing technique was used (Kaimal and Finnigan, 1994). As the lidar switched between two different scanning modes (vertical stare and DBS), the observed time series of vertical velocity, *w*, was discontinuous. The lidar *w* observations over a 2-hour period were split into two sets. The first set consisted of ~60 short records taken in vertical stare mode, each with ~28 samples approximately every 3.6 seconds from which the high frequency part of the spectrum was estimated by applying a Fourier Transform. Spectra were averaged to give a single high-frequency spectrum. A second set was made up of 240 non-overlapping block averages (each block containing 30 s of data) from which the low frequency part of the spectrum was estimated. Then the high and low frequency parts of the spectrum were combined and smoothed. The splicing method was tested on the continuous, BT Tower sonic anemometer time series by sampling it in a similar

way to the lidar and the resulting spectrum was found to agree well with the continuous data spectrum in magnitude.

2.3 The case.

Model behaviour has been analysed for the case of the 30th September 2011. This was the middle of a period of five warmer than average and completely cloud free days in the London area (28^{th} Sept – 2^{nd} Oct). These conditions were a result of high pressure to the east of the UK. This case has been studied by J F Barlow et al., (2015) as a strong Urban Heat Island event. An important aspect of the case for subsequent analysis is that there is a significant synoptic flow from the south. Data from the lidar situated at WCC shows that the boundary layer grows in depth during the morning, with convective overturning from approximately 1100 to 1600 UTC with this being deepest and most intense from 1400 to 1500 UTC (figure 4).

3. Overview of behaviour of model compared to observations

In this section we present some basic behaviour of the models and comparisons between the models and observations which serve as a starting point for the analysis in sections 4 and 5.

Figure 2(a) shows the 1.5m temperature field in U100 at 1400 UTC. The city is clearly warmer and some fine scale detail can be seen (e.g. parks and rivers colder) reflecting the high resolution surface information in the model. The cooler approximately east-west line to the south of the figure is the ridge of a range of hills (the North Downs). Figure 2(b) shows the vertical velocity field at 293m above the ground. Comparing with Figure 2(a) it is clear that there is stronger overturning over the densely urban areas around the centre of London. The other feature, which is noticeable, is that the morphology of the overturning is strongly

242 influenced by the southerly wind with many linear/elongated features being aligned roughly
243 along the flow. Such Horizontal Convective Rolls (LeMone, 1973) are common in sheared
244 convective boundary layers and it was suggested by Miao and Chen (2008) that they might be
245 common over urban surfaces where shear stress is higher. There are also signs of more
246 elongated features, in particular close to the inflow (southern) boundary of the domain.

247 Figure 3 introduces two key aspects of model behaviour, which will be the subject of later
248 sections of this paper. Figure 3(a) shows the horizontal vertical velocity field in U100 over
249 the subset of the domain that corresponds to the small 100m model. Figure 3(b) shows the
250 same field in the same subset of U50. It is noticeable to the eye that the features in the
251 vertical velocity field are smaller (both the width of the streaks of high vertical velocity and
252 their spacing). This immediately implies that the model is not converged in this respect. It is
253 important to understand the effects of this because of the practical question of at which grid-
254 length the model needs to be run for different applications. This aspect is discussed further in
255 Section 4. Figure 3(c) shows the whole domain of U100S. It is clear that there are significant
256 spin up effects as the air enters through the southern boundary of the model. These manifest
257 themselves as an area close to the boundary where there is no overturning (because the
258 driving model does not support it) but further into the model elongated along wind Horizontal
259 Convective Rolls (HCRs) are generated. Further downstream again (roughly north of an east-
260 west line half way between the north and south boundaries) the rolls become less coherent
261 and look more like the elongated features in the subset of the larger domain. The formation of
262 these rolls is discussed in Section 5 along with the practical implications of this spin up which
263 clearly extends about 15km into the domain in this case. The location of the measurements is
264 shown on Figure 3 (c) and was at the downstream end of the HCRs where they are starting to
265 break up.

Figure 4 shows time/height cross sections of vertical velocity at the location of the lidar. Figure 4(d) shows the vertical velocity from the lidar observations which show overturning in the mixed layer which deepens rapidly after 1200 UTC. The equivalent U50 and U100 data (Figures 4c and 4b) show similar overturning with, by eye, both the depth of the overturning and its magnitude in reasonably good agreement with the observations. The magnitude of the overturning appears somewhat weaker in the model and the frequency at which the overturning happens appears somewhat slower in the models and slower in U100 compared to U50. These comparisons of the model with observations are analysed more quantitatively below. U100S has similar overturning but at a much lower frequency and is clearly in poorer agreement with the observations. This is empirically understandable in the sense that if there are HCRs in the along wind direction in U100S (as shown in Figure 3) they would tend to advect along their length and so not change very rapidly when seen from a fixed point.

Figure 5 shows profiles of sensible heat flux in the U100 and U50 including the explicit fluxes corresponding to the explicit vertical velocities and the parameterised heat flux from the boundary layer scheme. The fluxes were calculated over a box 5x5km square centred at the BT Tower location. The explicit fluxes were calculated at a fixed time (1400 UTC) using the variations in potential temperature and vertical velocity across the box for each model level. In both models the flux is primarily carried explicitly except for close to the ground. As would be expected the U50 has the explicit flux increasing more quickly above the ground. Both profiles show a large entrainment peak at around 650m. This is consistent with the morning increase in the mixed layer height with time and also as the air flows over the urban area with higher heat fluxes.

Figure 6(a) shows profiles of vertical velocity variance calculated at the location of the lidar in the time domain from 1400-1500 for the U100, U50 and the lidar data. It is clear that the models both have significantly lower vertical velocity variance than is observed but with this

error smallest at the lowest levels. The low values of variance at low levels are probably a manifestation of being under-resolved (as discussed in section 5). It is notable that U50 has higher variance than U100 below 300m (where the comparisons with the BT tower in section 4 are made) but the variance is lower than U100 above that. U100 has a clear sign of a double structure with two separate peaks which can be seen by eye in figure 3 (as two separate levels at which the vertical velocity features tend to be centred). Figure 6(b) shows a horizontally averaged theta profile which shows that the double structure in the model corresponds to a stable layer around 700-900m altitude with a second less stable region above. It is notable that the variance in U50 is much lower than that in U100 in the region of the more elevated of the two peaks, to the degree that U50 doesn't have the peak at all.

Figure 7 shows the mixing height, z_{MH}, at the WCC measurement site as a function of time derived using a vertical velocity variance threshold of 0.1 $m^2 s^{-2}$ applied to both the lidar and model data. The error bars correspond to perturbing the threshold by ±30%. It should be noted that earlier in the day, the explicit vertical velocity variance in the model does not reach 0.1 $m^2 s^{-2}$ at any height, and thus z_{MH} could not be derived according to this threshold. However, from 1300 to 1500 UTC agreement is reasonably good for U100 although it is clear from the variance profiles shown in Figure 6(a) that the value of z_{MH} derived for the models will depend more strongly on the threshold chosen than in the case of the lidar. The somewhat lower value of z_{MH} derived for U50 reflects the lack of variance seen in Figure 6(a) in the elevated area of overturning from about 1000-1300m. This may result from the heat fluxes being somewhat lower than in reality due to the deficiencies in the surface exchange scheme in the model mentioned in section 2.1. The U100 model, in contrast has more significant variance between 1000-1300m because some of the larger scale structures are more energetic as can be seen in Figure 4.

4. Spectral behaviour and effect of resolution

In this section the effect of model resolution is analysed with comparisons between the spectra and turbulent lengthscales of U50, U100 and observations. As discussed above, figure 3 shows that the model vertical velocity fields are different at 50m compared to 100m grid-length with smaller horizontal scales appearing in the vertical velocity structures. In addition figure 4 shows that the overturning appears to be faster in the U50. In order to better understand these aspects, spectral analysis has been carried out. Figure 8 shows spectra of timeseries of vertical velocities, w, for the 14-16UTC time window. The figure includes spectra of w from the sonic anemometer on the BT Tower (height 190 m), the nearest lidar gate (mid-point 184 m) and model spectra calculated for the nearest model level (midpoint height 192 m) and gridpoint. The spectral energy density has been multiplied by the frequency to highlight the most energetic scales.

The sonic anemometer spectra from the BT Tower and the lidar data agree that the peak frequency is around $2x10^{-3}$ Hz although there is somewhat less energy in the lidar spectrum. This difference is discussed by Barlow et al., (2015) and is thought to be related to the differences in sampling frequency, sampling volume and location of the two instruments. The U50 and U100 spectra have similar peak magnitude of scaled spectral energy density compared to the observations. As variance is given by integrating the spectral energy density with frequency the spectra are consistent with this in that the variance at 190m in figure 6 is higher in U50. There is a sharp drop-off in energy at higher frequencies due to the finite resolution of the model. This starts near the peak frequency for U50, and is below the peak frequency for U100. U50 therefore is close to resolving the dominant frequency whereas U100 only partially resolves the peak. This is consistent with the finding that, in the spatial domain, the spacing of the high vertical velocity features appears to reduce between U100

and U50 which means that U100 is not completely resolving the structures. It is also consistent with the variance data shown in Figure 6 where U50 is closer to having the observed variance at 190m. By comparison, Miao et al., 2008) used the WRF model running with 500m grid-length over Beijing and found HCRs of a smaller aspect ratio than for rural boundary layers: it is possible that their structures were under-resolved. The implication is that, with the MetUM, a grid-length of about 50m is required to resolve the most important spatial/temporal structures in this convective boundary layer although, as shown in figure 5, 100m may still be sufficient if we are only concerned with bulk properties such as heat flux averaged across a certain distance. The numbers quoted in the previous sentence will be different with different models with different dynamical cores. From figure 8 we can also estimate what the spectra for hypothetical 25m and 12.5m models would look like assuming that each factor of two resolution will again give a factor of two increase in the frequency at which the model energy drops off from the observational data. A 25m model would more comfortably resolve the most energetic frequencies and we might expect more convergence in the comparison with observations at shorter grid-lengths than this. This is based only from extrapolating what we see in the spectra of the 100m and 50m models so experiments at 25m and also probably at 12.5m would be needed to confirm this conclusion.

Given the nature of the observational data (time series in one location) the spectra discussed above were computed in the time domain. As a check we also calculated a spectrum for U50 in the space domain from the horizontal field along the transect. If the spatial frequencies in this spectrum are converted into temporal ones using the wind velocity (about $6ms^{-1}$ at BT Tower level) the spectrum (not shown) looks very similar to the U50 one in figure 8. This implies that the behaviour of the time spectrum is dominated by advection of spatial features rather than the temporal changes in these. This fits with the observation that the drop off in the U100 and U50 spectra occur at about a factor of 2 different frequency which corresponds

365 in the difference in spatial resolution (whereas, as shown in table 1, the timestep is a factor of
366 3 different). If converted to a lengthscale with the wind velocity the frequency at which the
367 model curve starts to strongly drop away from observed values (around $2x10^{-2}s^{-1}$
368 corresponding to 50s for U100) corresponds to a length of around 6 grid-lengths using the
369 advection speed mentioned above. This is the magnitude of filter scale typically seen in NWP
370 models (Lean et al., 2003). In contrast in the temporal domain the same frequency at which
371 the model starts to be attenuated is much lower (50x) than the Nyquist frequency due to the
372 timestep , $1.0s^{-1}$. This implies that the model is running with a shorter timestep than needed to
373 resolve this convective overturning. In practice it is found that this short a timestep is
374 required for the model to be numerically stable but this requirement may well not come from
375 the boundary layer in the centre of the domain. It could come, for example, from higher up in
376 the model (which extends to 40km) or from the region of the boundaries.

377 The analysis above applies to only one level, 190m above ground, which is where the BT
378 tower measurements were taken. However, the lidar data also allows spectra to be calculated
379 at a number of heights, and a dominant time-scale, Λ_t, can be estimated from the frequency of
380 the peak. The spectral energy peak was estimated by fitting a second-order polynomial
381 (Wood et al. 2010). The dominant length-scale $\Lambda_x = U\,\Lambda_t$ was calculated at each height using
382 the observed hourly mean wind profile, *U(z)*. The same calculation was done for the model
383 spectra, using wind profiles spatially averaged over a 10km box around the observation site.
384 Fig. 9 shows the height-normalised profile of dominant lengthscales, all of which have been
385 scaled using z_{MH} for lidar and model data. The empirical relationship due to Caughey and
386 Palmer (1979) (CP) has also been added as a reference for a classical Convective Boundary
387 Layer. The general trend of the lidar data follows the CP relationship, and the magnitude is
388 slightly smaller but with two large peaks superimposed. The two peaks are consistent with
389 the double structure in the overturning discussed in section 3. The models both have longer

lengthscales than the lidar observations which corresponds to the limited resolution as discussed above. Closer to the ground the models have larger scales relative to the observations. The resolution effect is clear in that the U100 data generally has a larger lengthscale than U50. U50 shows a weak double peak structure whereas U100 shows a single lower peak which is lower than the peaks in the observations. These results demonstrate again that U50 is producing near-realistic convective structures and even U100 is producing structures that are only 2-3 times the expected scale at a height of around $z_{MH}/2$.

5. Horizontal behaviour and spin up.

It is also of interest to look at the spatial distribution of some of the quantities discussed in section 3. Although we do not have any observational data on horizontal variability it is important to understand the effect of the city surface and spin up at the edge of the model domain.

Figure 10 shows a cross section of instantaneous vertical velocity at 1400 UTC U100. The cross section is along a transect from south to north, i.e. aligned with the wind, across the U100 domain passing through the location of the BT tower (i.e. along the dotted line shown in figure 3c). The overturning can be clearly seen and it behaves as would be expected with the depth of the overturning increasing as the air flows over the built up area of London and decreasing again downstream of the city. This is summarised in Figure 11(a) which shows the mixing height (solid line) calculated from a spatial variance threshold of 0.1 m^2s^{-2} along with the model urban fraction averaged over gridpoints in a 5km box surrounding each point. It is striking that the mixing height is very flat over the city despite the fact that the urban fraction and surface heat flux (not shown) both have peaks corresponding to the centre of the city. This is assumed to be because of a synoptically imposed inversion (which can be seen from

the potential temperature (theta) contours in figure 10 and figure 6b) which caps the height of the overturning. Figure 10 shows evidence of the double structure in the vertical as seen in the variance values (Figure 6) - vertical velocity features can be seen which are centred in the vertical at relatively low levels (~400m) while others are evident higher up (~1000m). The sudden reduction of the depth of overturning at 60km on the transect visible in figures 10 and 11a which subsequently recovers before 80km may be partly due to a region of a relatively low inversion at around 600m visible in the theta field.

It is important to understand spin up effects at the edge of the domains and, in particular, how far they extend into the domain. Given the expense of running high resolution models it is important not to run domains larger than are strictly required for the application for which they are intended.

The discussion around Figure 3 introduced the elongated roll structures, HCRs, aligned along the wind direction, when air flows into the domain of U100S. Similar, but less pronounced, HCRs may also be seen near the inflow boundary of U100 (Figure 2b). HCRs such as this can be valid meteorological phenomena (e.g. when generated as air comes over a coast or other physical boundary) but are very likely to be spurious when generated by the boundary of a model. The boundary conditions of the 100m grid-length models come from a lower resolution model (500m) which are only updated every 15 minutes. It would therefore not be possible for explicit overturning in the boundary layer to be propagated into the model from the boundaries. This results in a region of no overturning close to the boundary, followed by the HCRs further into the domain which then break up into more realistic looking structures further downstream. These effects represent spin up as the behaviour of the modelled air adjusts to the high resolution. HCRs due to spin up at the inflow boundary have been seen in a number of contexts in turbulence permitting models (Boutle et al., 2014, Hanley et al., 2015). In this section we analyse why these rolls are seen.

In order to quantify the spin up effects, Figure 12 shows an analysis of the aspect ratio of objects in the vertical velocity field on the 290m model level with the objects being defined as contiguous areas with vertical velocity greater than $2ms^{-1}$. The aspect ratio was calculated using a least squares method to fit an ellipse to each object and then determine the aspect ratio as the ratio of major to minor axis of the fitted ellipse. For each object in the whole domain the aspect ratio and distance from the inflow (southern) boundary was calculated. The aspect ratio was then plotted as a function of distance from the boundary with some smoothing (moving box of 30 gridpoints which corresponds to 3km). The figure shows that, in U100, even in the centre of the domain the high vertical velocity objects are somewhat elongated with average aspect ratio around 3.0 (as can be seen by eye in figure 3a). In that model there is a clear tendency for more elongated objects close to the inflow boundary with average aspect ratio increased to around 6.0. However, the curve U100S shows much more elongated cells with the average aspect ratio peaking at nearly 10.0. It is clear that the spin up effect in terms of HCRs is more pronounced when the boundary of the domain is closer to the region with strong overturning.

In order to understand this in more detail an analysis based on the boundary layer stability parameter is presented. Salesky et al., 2017) carried out LES studies of the transition between roll and cellular organisation in convective boundary layers. They found that the transition could be described by a stability parameter, $-z_i/L$ where z_i is the inversion height and L is the Obukhov length. We assume that $z_i = z_{MH}$ at the time of the analysis (1400 UTC) in the middle of the day. It was found that the transition takes place at around $-z_i/L = 10$ with smaller values of $-z_i/L$ giving more roll like structures and higher values more cellular. In this case we do not see cells due to the relatively strong synoptic flow, however we are interested in the transition between HCRs and more discrete (although still somewhat elongated) objects. It should be noted that the same 100m model does produce cellular

structures in convective boundary layers for other cases where there are much lighter winds (not shown).

Figure 11 shows the results for calculating the stability parameter along the same south-north transect used in figure 10. All quantities in this figure are averaged over 5km boxes centred on points along the transect. Figure 11(a) shows the mixing height calculated as a variance threshold for both the 100m and the small 100m models. In the small model the mixing height starts very small at the southern boundary but increases rapidly as the air transits the model domain. This is consistent with convection being driven by surface fluxes and so the overturning grows upwards from the surface once the air enters a model that is able to support it. Figure 11(b) shows the Obukhov Length, L, for both models. This was calculated (assuming unstable conditions) as $L=z/R_i$ (Businger et al., 1971) where R_i is the gradient Richardson number in the surface layer given by:

$$Ri = \frac{g\,\partial\bar{\theta}/\partial z}{\bar{\theta}\left(\partial\bar{U}/\partial z\right)^2}$$

R_i was calculated from the model data by fitting logarithmic polynomials to the smoothed (lengthscale 5km) θ and U profiles using the lowest 5 model levels (up to about 20m) and then using the fitted profiles to calculate the vertical derivatives. When the stability parameter, $-z_{MH}/L$, is calculated (figure 11c) the value is much lower in U100S, close to the southern boundary, than in U100, which is consistent with rolls being more prominent in U100S in that location. As the northern boundary of U100S is approached, the values are almost the same which implies that, by this point, the spin up effects are no longer important. Figure 11 also gives some insight into the reasons for this. Figure 11b shows the Obkuhov length along the transect. It is noticeable that L is small north of 65km on the transect despite the fact that the heat flux would be expected to be lower outside the urban area. This is

consistent with the low level shear being lower in this area as can be seen on cross sections of the wind strength (not shown). The values of the Obkuhov length are similar between the small and large models along the whole part of the transect that is inside the small model domain. Most of the difference in the stability parameter appears, therefore, to come from the difference in the mixing height. The boundary layer is more shear dominated in U100S near the boundary because it is shallower.

It is also noticeable in figure 11c that the stability parameter is also small near the boundary of U100 and that there is likely to be a similar spin up distance. This can be seen by eye in the vertical velocity fields (e.g. figure 2b) although the rolls are much weaker due to the lower surface heat flux outside the city.

Beyond the spin up zone it is striking to note that from 20-40 km, the Obukhov length remains near constant despite a large increase in urban fraction, as concurrent increases in both sensible heat flux and surface stress towards the city centre produce little overall change in surface layer stability. Together with the near constant mixing height over this zone, the boundary layer stability also remains near constant. The aspect ratio of convective structures stays fairly constant, reducing only slightly over 40-60km as the boundary layer stability parameter drops. The surprise is that the convective field remains relatively invariant despite massive changes in the urban surface, although this particular combination of increasing surface stress and heat flux might be peculiar to London, and the strong capping inversion across the region at the time.

Figures 3, 11 and 12 show that the spin up effects penetrate at least 10-15km into the domain of the U100S in this case although this distance will depend on the wind strength. It is interesting to note that in the spectral analysis in the section 4 the dominant timescale of the overturning, from the peak of the spectrum of the U100 in figure 8 is approximately 500s. If

511 one assumes the wind speed is about 10ms^{-1} (representative of the middle of the boundary
512 layer) this means that the spin up distance corresponds to 2-3 turnover times which seems
513 intuitively reasonable. U50 would be expected to have a somewhat shorter dominant
514 timescale from better resolving the peak in the observed spectrum and would therefore spin
515 up more quickly (although slower in terms of number of gridpoints). It is important to note
516 that while we have analysed these effects in terms of the stability parameter the details of
517 how far the spin up penetrates into the domain will depend on the model numerics and the
518 sub-grid mixing configuration employed. The effect of these two aspects of models on
519 convective structures were analysed in terms of an effective viscosity by Piotrowski et al.,
520 2009.

521 As shown in figure 4, these spin up artefacts can significantly degrade the model performance
522 compared to observations. This is an important issue for practical models with these
523 resolutions. The simple solution of simply extending the domain is not always feasible due to
524 the computational expense. One approach which was employed by Vosper et al., (2013) is to
525 use a variable resolution model. The benefits of variable resolution are discussed by Tang et
526 al., (2013) and Davies, (2017) although not in the particular context of the turbulence
527 permitting regime. The idea would be to extend the domain at lower resolution which can
528 help to push the spin up region further away from the area of interest at lower expense than
529 extending the domain at full resolution. A second possibility is to inject noise into the
530 boundary data to help the turbulent motions spin up. Variations on this approach have been
531 investigated by a number of workers including Muñoz-Esparza et al., (2014) and Mayor et
532 al., (2002). There are also approaches to this issue that have been developed within the CFD
533 community, for example running an auxillary model to model the inflow field as reported by
534 Lund et al., (1998).

It is clear that the effects of spin up and how far it penetrates into the domain will vary greatly according to the meteorological situation and so the importance of this, and the need for mitigation, will depend on the application of the particular model. So, for example, a model whose primary aim is to forecast fog (as in Boutle et al., 2016) will generally be of greatest utility in relatively low wind situations so spin up effects would be likely to be less of an issue.

6. Conclusions

A comparison has been presented between O(100m) grid-length versions of the MetUM over London and observations for a case of a cloud free convective boundary layer with a significant southerly wind. The boundary layer overturning is, in general, well represented in terms of the magnitude and depth of the overturning being in good agreement with vertical stare Doppler lidar observations of vertical velocity and the variation of these through the day.

An important practical question is the resolution requirements of the model. In order to help understand this the 100m model was compared to a 50m one. In both the 100m and 50m models most of the heat flux (except very close to the surface) is carried explicitly by overturning motions and is consistent between the two. This would imply that the turbulence is well resolved. In contrast, however, the comparison of the vertical velocity fields by eye reveals that the vertical features in the model are generally smaller in horizontal extent in the 50m model which implies that the models have not converged with resolution as far as horizontal size of structures is concerned. Spectral analysis in the time domain has been carried out to compare the model to observations from an anemometer at the top of the BT

559 tower and from the lidar. The models both represent the most energetic eddies without too
560 much attenuation but the 50m model represents significantly more frequencies higher than
561 the peak. The exact details of the spectra of the model compared to observations are likely to
562 depend on the model employed (dynamical core and sub-grid mixing) and the meteorological
563 situation. Vertical profiles of integral lengthscales were calculated using the lidar and model
564 data and showed that the most energetic eddies in the models are 2-3 times larger than the
565 lidar, and worse close to the ground, which implies that higher resolutions would be
566 preferable. The above indicates that, even at 50m resolution, the horizontal structures in the
567 convective overturning are under-resolved in the model. However, if only bulk properties
568 (e.g. heat fluxes, spatially averaged mixing height etc) are of interest models the implication
569 of this study is that the 100m model will have usable performance. It would be interesting in
570 future to extend the study to higher resolution models to see where convergence of the
571 horizontal structures is reached. This was not possible in the current study due to
572 computational constraints.

573 Although comparison with the available observations does not shed light on the spatial
574 variation of the mixing height, this also looks reasonable in the model with a deeper mixing
575 height over the more densely packed urban area in the centre of London. Comparison of the
576 80x80km domain 100m model of the London area with a much smaller 30x30km domain
577 model has allowed us to investigate spin up effects at the inflow boundary. These manifest
578 themselves as along wind rolls just downstream of the inflow boundary which then break up
579 approximately 10-15 km further downstream. In the case of the small model these rolls
580 extend almost half way across the domain and cause significantly poorer agreement, in terms
581 of temporal variation of vertical velocity, with the lidar vertical velocity observations. An
582 analysis has been carried out based on a boundary layer stability parameter calculated as the
583 ratio of the mixing height to the Obukhov Length. This implies that the formation of rolls is

584 primarily due to the small value of the mixing height near the inflow boundary (that
585 subsequently increases downstream towards more physically realistic values), causing the
586 boundary layer to be shear dominated. These spin up effects are likely to be an intrinsic
587 property of these models and therefore may need to be avoided by using larger domains (or
588 variable resolution) in order to push the area of interest further away from the boundary. An
589 alternative approach may be to inject noise into the model via the boundaries in order to help
590 the turbulence spin up more quickly.

591

592

593 Acknowledgements.

594 Observations were obtained under the ACTUAL project which was funded under
595 Engineering and Physical Sciences Research Council grant number EP/G022938/1. The
596 authors would like to thank Heather Guy for developing the ellipse fitting method used.

597 The authors would also like to thank the two anonymous reviewers whose comments helped
598 improve the paper.

References

Allen, L., Lindberg, F., & Grimmond, C. S. B. (2011). Global to city scale urban anthropogenic heat flux: Model and variability. *International Journal of Climatology*, *31*(13), 1990–2005. https://doi.org/10.1002/joc.2210

Barlow, J., Best, M., Bohnenstengel, S. I. S. I., Clark, P., Grimmond, S., Lean, H., … Zhong, J. (2017). Developing a research strategy to better understand, observe, and simulate urban atmospheric processes at Kilometer to Subkilometer Scales. *Bulletin of the American Meteorological Society*, *98*(10), ES261-ES264. https://doi.org/10.1175/BAMS-D-17-0106.1

Barlow, J. F., Halios, C. H., Lane, S. E., & Wood, C. R. (2015). Observations of urban boundary layer structure during a strong urban heat island event. *Environmental Fluid Mechanics*, *15*(2), 373–398. https://doi.org/10.1007/s10652-014-9335-6

Barlow, J. F., Harrison, J., Robins, A. G., & Wood, C. R. (2011). A wind-tunnel study of

flow distortion at a meteorological sensor on top of the BT Tower, London, UK. *Journal of Wind Engineering and Industrial Aerodynamics*, *99*(9), 899–907. https://doi.org/10.1016/j.jweia.2011.05.001

Best, M, J., M, P., Clark, D, B., Rooney, G, G., Essery, R, L, H., Menard C, B., … Harding, R. J. (2011). The Joint UK Land Environment Simulator (JULES), Model Description - Part 1 : Energy and Water Fluxes The Joint UK Land Environment Simulator (JULES), model description – Part 1 : Energy and water fluxes, 677–699. https://doi.org/10.5194/gmd-4-677-2011

Best, M. J. (2005). Representing urban areas within operational numerical weather prediction models. *Boundary Layer Meteorology*, *114*, 91–109. https://doi.org/10.1007/s10546-004-4834-5

Best, M. J., & Grimmmmond, C. S. B. (2015). Key conclusions of the first international urban land surface model comparison project. *Bulletin of the American Meteorological Society*, *96*(5), 805–819. https://doi.org/10.1175/BAMS-D-14-00122.1

Bohnenstengel, S. I., Evans, S., Clark, P. a., & Belcher, S. E. (2011). Simulations of the London urban heat island. *Quarterly Journal of the Royal Meteorological Society*, *137*(659), 1625–1640. https://doi.org/10.1002/qj.855

Bohnenstengel, S. I., Hamilton, I., Davies, M., & Belcher, S. E. (2014). Impact of anthropogenic heat emissions on London's temperatures. *Quarterly Journal of the Royal Meteorological Society*, *140*, 687–698. https://doi.org/10.1002/qj.2144

Boutle, I. A., Eyre, J. E. J., & Lock, A. P. (2014). Seamless Stratocumulus Simulation across the Turbulent Gray Zone. *Monthly Weather Review*, *142*(4), 1655–1668. https://doi.org/10.1175/MWR-D-13-00229.1

Boutle, I. A., Finnenkoetter, A., Lock, A. P., & Wells, H. (2016). The London Model: Forecasting fog at 333 m resolution. *Quarterly Journal of the Royal Meteorological Society*, *142*(694), 360–371. https://doi.org/10.1002/qj.2656

Businger, J. A., Wyngaard, J. C., Izumi, Y., & Bradley, E. F. (1971). Flux-Profile Relationships in the Atmospheric Surface Layer. *Journal of the Atmospheric Sciences*. https://doi.org/10.1175/1520-0469(1971)028<0181:FPRITA>2.0.CO;2

Caughey, S. J., & Palmer, S. G. (1979). Some aspects of turbulence structure through the depth of the convective boundary layer. *Quarterly Journal of the Royal Meteorological Society*, *105*(446), 811–827. https://doi.org/10.1002/qj.49710544606

Chen, F., Kusaka, H., Bornstein, R., Ching, J., Grimmond, C. S. B., Grossman-Clarke, S., … Zhang, C. (2011). The integrated WRF/urban modelling system: development, evaluation, and applications to urban environmental problems. *International Journal of Climatology*, *31*(2), 273–288. https://doi.org/10.1002/joc.2158

Ching, J., Rotunno, R., LeMone, M., Martilli, A., Kosovic, B., Jimenez, P. A., & Dudhia, J. (2014). Convectively Induced Secondary Circulations in Fine-Grid Mesoscale Numerical Weather Prediction Models. *Monthly Weather Review*, *142*(9), 3284–3302. https://doi.org/10.1175/MWR-D-13-00318.1

Clark, P., Roberts, N., Lean, H., Ballard, S. P., & Charlton-Perez, C. (2016). Convection-permitting models: A step-change in rainfall forecasting. *Meteorological Applications*, *23*(2). https://doi.org/10.1002/met.1538

Davies, T. (2017). Dynamical downscaling and variable resolution in limited-area models. *Quarterly Journal of the Royal Meteorological Society*, *143*(702), 209–222. https://doi.org/10.1002/qj.2913

Davies, T., Cullen, M. J. P., Malcolm, A. J., Mawson, M. H., Staniforth, A., White, A. A., & Wood, N. (2005). A new dynamical core of the Met Office's global and regional modelling of the atmosphere. *Quarterly Journal of the Royal Meteorological Society*, *131*(608), 1759–1782. https://doi.org/10.1256/qj.04.101

Efstathiou, G. A., & Beare, R. J. (2015). Quantifying and improving sub-grid diffusion in the boundary-layer grey zone. *Quarterly Journal of the Royal Meteorological Society*, *141*(693), 3006–3017. https://doi.org/10.1002/qj.2585

Efstathiou, G. A., Beare, R. J., Osborne, S., & Lock, S. A. P. (2016). Grey zone simulations of the morning convective boundary layer development. *Journal of Geophysical Research*, *121*(9), 4769–4782. https://doi.org/10.1002/2016JD024860

Halios, C. H., & Barlow, J. F. (2018). Observations of the Morning Development of the Urban Boundary Layer Over London, UK, Taken During the ACTUAL Project. *Boundary-Layer Meteorology*, *166*(3), 395–422. https://doi.org/10.1007/s10546-017-0300-z

Hanley, K. E., Barrett, A. I., & Lean, H. W. (2016). Simulating the 20 May 2013 Moore, Oklahoma tornado with a 100-metre grid-length NWP model. *Atmospheric Science Letters*, *17*(8). https://doi.org/10.1002/asl.678

Hanley, K. E., Plant, R. S., Stein, T. H. M., Hogan, R. J., Nicol, J. C., Lean, H. W., … Clark, P. A. (2015). Mixing-length controls on high-resolution simulations of convective storms. *Quarterly Journal of the Royal Meteorological Society*, *141*(686). https://doi.org/10.1002/qj.2356

Helfter, C., Famulari, D., Phillips, G. J., Barlow, J. F., Wood, C. R., Grimmond, C. S. B., & Nemitz, E. (2011). Controls of carbon dioxide concentrations and fluxes above central London. *Atmospheric Chemistry and Physics*, *11*(5), 1913–1928. https://doi.org/10.5194/acp-11-1913-2011

Holt, T., & Pullen, J. (2007). Urban Canopy Modeling of the New York City Metropolitan Area: A Comparison and Validation of Single- and Multilayer Parameterizations. *Monthly Weather Review*, *135*(5), 1906–1930. https://doi.org/10.1175/MWR3372.1

Honnert, R., Masson, V., & Couvreux, F. (2011). A Diagnostic for Evaluating the Representation of Turbulence in Atmospheric Models at the Kilometric Scale. *Journal of the Atmospheric Sciences*, *68*(12), 3112–3131. https://doi.org/10.1175/JAS-D-11-061.1

Kaimal, J. C., & Finnigan J. J. (1994). *Atmospheric boundary layer flows—their structure and measurement*. Oxford University Press.

Kendon, E. J., Roberts, N. M., Fowler, H. J., Roberts, M. J., Chan, S. C., & Senior, C. A. (2014). Heavier summer downpours with climate change revealed by weather forecast resolution model. *Nature Climate Change*, *4*(7), 570–576. https://doi.org/10.1038/nclimate2258

Lane, S. E., Barlow, J. F., & Wood, C. R. (2013). An assessment of a three-beam Doppler lidar wind profiling method for use in urban areas. *Journal of Wind Engineering and*

Industrial Aerodynamics, *119*, 53–59. https://doi.org/10.1016/j.jweia.2013.05.010

Lean, H. W., & Clark, P. A. (2003). The effects of changing resolution on mesocale modelling of line convection and slantwise circulations in FASTEX IOP16. *Quarterly Journal of the Royal Meteorological Society*, *129*(592 PART A). https://doi.org/10.1256/qj.02.57

LeMone, M. (1973). The structure and dynamics of horizontal roll vortices in the planetary boundary layer. *Journal of Atmospheric Science*, *30*, 1077–1091.

Leroyer, S., Bélair, S., Husain, S. Z., & Mailhot, J. (2014). Subkilometer numerical weather prediction in an urban coastal area: A case study over the vancouver metropolitan area. *Journal of Applied Meteorology and Climatology*, *53*(6), 1433–1453. https://doi.org/10.1175/JAMC-D-13-0202.1

Lock, A. P., Brown, A. R., Bush, M. R., Martin, G. M., & Smith, R. N. B. (2000). A New Boundary Layer Mixing Scheme. Part I: Scheme Description and Single-Column Model Tests. *Monthly Weather Review*, *128*(9), 3187–3199. https://doi.org/10.1175/1520-0493(2000)128<3187:ANBLMS>2.0.CO;2

Lund, T. S., Wu, X., & Squires, K. D. (1998). Generation of inflow data for spatially-developing turbulent boundary layer simulations. *Journal of Computational Physics*, *144*, 233. https://doi.org/DOI 10.1006/jcph.1998.5882

Mayor, S. D., Spalart, P. R., & Tripoli, G. J. (2002). Application of a Perturbation Recycling Method in the Large-Eddy Simulation of a Mesoscale Convective Internal Boundary Layer. *Journal of the Atmospheric Sciences*, *59*(1995), 2385–2395. https://doi.org/10.1175/1520-0469(2002)059<2385:AOAPRM>2.0.CO;2

Miao, S., & Chen, F. (2008). Formation of horizontal convective rolls in urban areas. *Atmospheric Research*, *89*(3), 298–304. https://doi.org/10.1016/j.atmosres.2008.02.013

Miao, S., Chen, F., LeMone, M. a., Tewari, M., Li, Q., & Wang, Y. (2009). An Observational and Modeling Study of Characteristics of Urban Heat Island and Boundary Layer Structures in Beijing. *Journal of Applied Meteorology and Climatology*, *48*(3), 484–501. https://doi.org/10.1175/2008JAMC1909.1

Muñoz-Esparza, D., Kosović, B., Mirocha, J., & van Beeck, J. (2014). Bridging the Transition from Mesoscale to Microscale Turbulence in Numerical Weather Prediction Models. *Boundary-Layer Meteorology*, *153*(3), 409–440. https://doi.org/10.1007/s10546-014-9956-9

Nicol, J. C., Hogan, R. J., Stein, T. H. M., Hanley, K. E., Clark, P. A., Halliwell, C. E., … Plant, R. S. (2015). Convective updraught evaluation in high-resolution NWP simulations using single-Doppler radar measurements. *Quarterly Journal of the Royal Meteorological Society*, *141*(693). https://doi.org/10.1002/qj.2602

Piotrowski, Z. P., Smolarkiewicz, P. K., Malinowski, S. P., & Wyszogrodzki, A. A. (2009). On numerical realizability of thermal convection. *Journal of Computational Physics*, *228*(17), 6268–6290. https://doi.org/10.1016/j.jcp.2009.05.023

Prein, A. F., Langhans, W., Fosser, G., Ferrone, A., Ban, N., Goergen, K., … Leung, R. (2015). A review on regional convection-permitting climate modeling: Demonstrations, prospects, and challenges. *Reviews of Geophysics*, *53*(2), 323–361. https://doi.org/10.1002/2014RG000475

Ronda, R. J., Steeneveld, G. J., Heusinkveld, B. G., Attema, J. J., & Holtslag, A. A. M. (2017). Urban finescale forecasting reveals weather conditions with unprecedented detail. *Bulletin of the American Meteorological Society*, *98*(12), 2675–2688. https://doi.org/10.1175/BAMS-D-16-0297.1

Salesky, S. T., Chamecki, M., & Bou-Zeid, E. (2017). On the Nature of the Transition Between Roll and Cellular Organization in the Convective Boundary Layer. *Boundary-Layer Meteorology*, *163*(1), 41–68. https://doi.org/10.1007/s10546-016-0220-3

SMAGORINSKY, J. (1963). General Circulation Experiments With the Primitive Equations. *Monthly Weather Review*, *91*(3), 99–164. https://doi.org/10.1175/1520-0493(1963)091<0099:GCEWTP>2.3.CO;2

Stein, T. H. M., Hogan, R. J., Clark, P. A., Halliwell, C. E., Hanley, K. E., Lean, H. W., … Plant, R. S. (2015). The Dymecs project: A Statistical approach for the evaluation of convective storms in high-resolution NWP models. *Bulletin of the American Meteorological Society*, *96*(6). https://doi.org/10.1175/BAMS-D-13-00279.1

Stein, T. H. M., Hogan, R. J., Hanley, K. E., Nicol, J. C., Lean, H. W., Plant, R. S., … Halliwell, C. E. (2014). The three-dimensional morphology of simulated and observed convective storms over Southern England. *Monthly Weather Review*, *142*(9). https://doi.org/10.1175/MWR-D-13-00372.1

Tang, Y., Lean, H. W., & Bornemann, J. (2013). The benefits of the Met Office variable resolution NWP model for forecasting convection. *Meteorological Applications*, *20*(4). https://doi.org/10.1002/met.1300

Vosper, S., Carter, E., Lean, H., Lock, A., Clark, P., & Webster, S. (2013). High resolution modelling of valley cold pools. *Atmospheric Science Letters*, *14*(3). https://doi.org/10.1002/asl2.439

Wilson, D. R., & Ballard, S. P. (1999). A microphysically based precipitation scheme for the UK Meteorological Office Unified Model. *Quarterly Journal of the Royal Meteorological Society*, *125*(557), 1607–1636. https://doi.org/10.1256/smsqj.55706

Wood, C. R., Lacser, a., Barlow, J. F., Padhra, a., Belcher, S. E., Nemitz, E., … Grimmond, C. S. B. (2010). Turbulent Flow at 190 m Height Above London During 2006–2008: A Climatology and the Applicability of Similarity Theory. *Boundary-Layer Meteorology*, *137*(1), 77–96. https://doi.org/10.1007/s10546-010-9516-x

Wyngaard, J. C. (2004). Toward Numerical Modeling in the "Terra Incognita." *Journal of the Atmospheric Sciences*, *61*(14), 1816–1826. https://doi.org/10.1175/1520-0469(2004)061<1816:TNMITT>2.0.CO;2

Figure Captions

Figure 1. Map of urban fraction used in the U100. The whole area shown is the 80 x 80 km domain used for U100 and U50. The smaller square shows the area of the 30 x 30 km domain of U100S. Also shown is the location of the observations – at this scale both the BT Tower and WCC are close to the tip of the arrow in the central area.

Figure 2 (a) 1.5m temperature field at 1400 UTC on the U100 domain. (b) Vertical velocity at 293m on the same domain.

Figure 3. Vertical velocity at 293m in (a) U100, (b) U50 and (c) U100S. In all cases the area shown is that of the domain of U100S. The North-South dotted line in (c) represents the location of the transect used in Figures 10 and 11 and the centre of the circle on the transect is the location of the BT tower (WCC close by on this scale). The scale to the right of (c) represents locations in km on the transect comparable to those on Figures 10 and 11.

Figure 4. Time/height cross sections of vertical velocity at WCC in (a) U100S (b) U100, (c) U50 and (d) lidar observations.

Figure 5. Profiles of sensible heat flux in U100 (left) U50. Dotted lines are parameterised flux, solid is explicit and dashed is total.

Figure 6. (a) Vertical velocity variance profiles from 1300-1400 UTC. Sold line is lidar data, dashed is U100 and dotted is U50 (b) theta profile in U100 and U50 averaged over a 2km box centred on the BT tower.

Figure 7. Mixing height at WCC as a function of time from lidar observations, U100 and U50. The mixing height was calculated using a variance threshold of 0.1 m^2s^{-2}.The solid line is lidar data, circles/dotted U100 and plus signs/dashes U50. Error bars were calculated by perturbing the variance threshold up and down by 30%.

Figure 8. Spectra for U100 and U50 compared to lidar and BT tower observations. Plus signs/sold lines BT tower, triangles/dashed lines lidar, diamonds/dash-dot U50 and squares/dotted lines U100.

Figure 9. Turbulence lengthscale as a function of height, both normalised by mixing height. Solid line is lidar data, dotted line from U50, dashed line from U100 and dash-dot line from Caughey et al., 1979.

Figure 10. Cross section of vertical velocity field (shading) and potential temperature (theta) contours in U100 at 1400 UTC along south (left) to north transect through BT tower with orography also shown.

Figure 11. South to north transect through BT tower showing urban fraction (dotted line) and plots for U100 (solid line) and U100S (dashed line). (a) mixing heights, (b) obukhov length (absolute value), (c) stability parameter.

Figure 12. Aspect ratio of vertical velocity objects as a function of distance from the southern boundary of the domain for U100 and U100S (dashed line) 100m model. A vertical velocity threshold of 2.0 ms^{-1} was used on a vertical velocity field on model level 20 (290m above ground). The aspect ratio data was smoothed as a function of distance from the southern boundary using an averaging length of 3km.

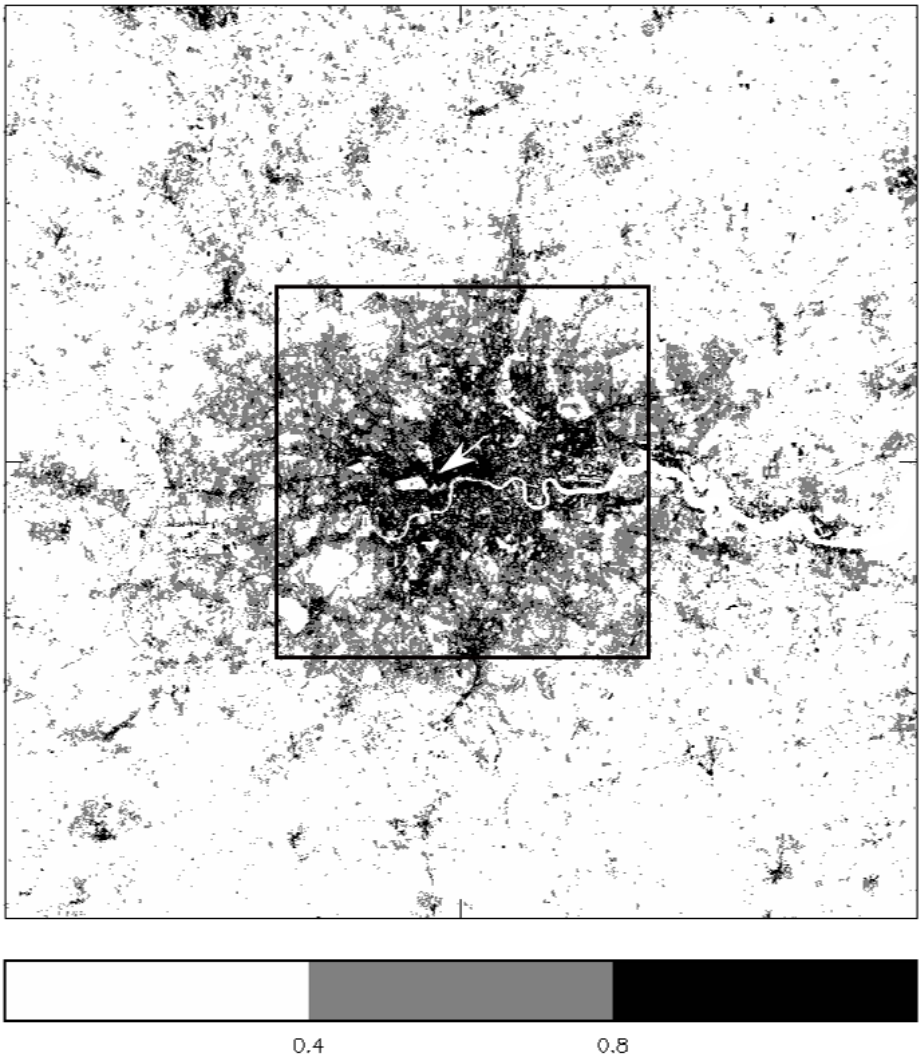

Figure 1. Map of urban fraction used in the U100. The whole area shown is the 80 x 80 km domain used for U100 and U50. The smaller square shows the area of the 30 x 30 km domain of U100S. Also shown is the location of the observations – at this scale both the BT Tower and WCC are close to the tip of the arrow in the central area.

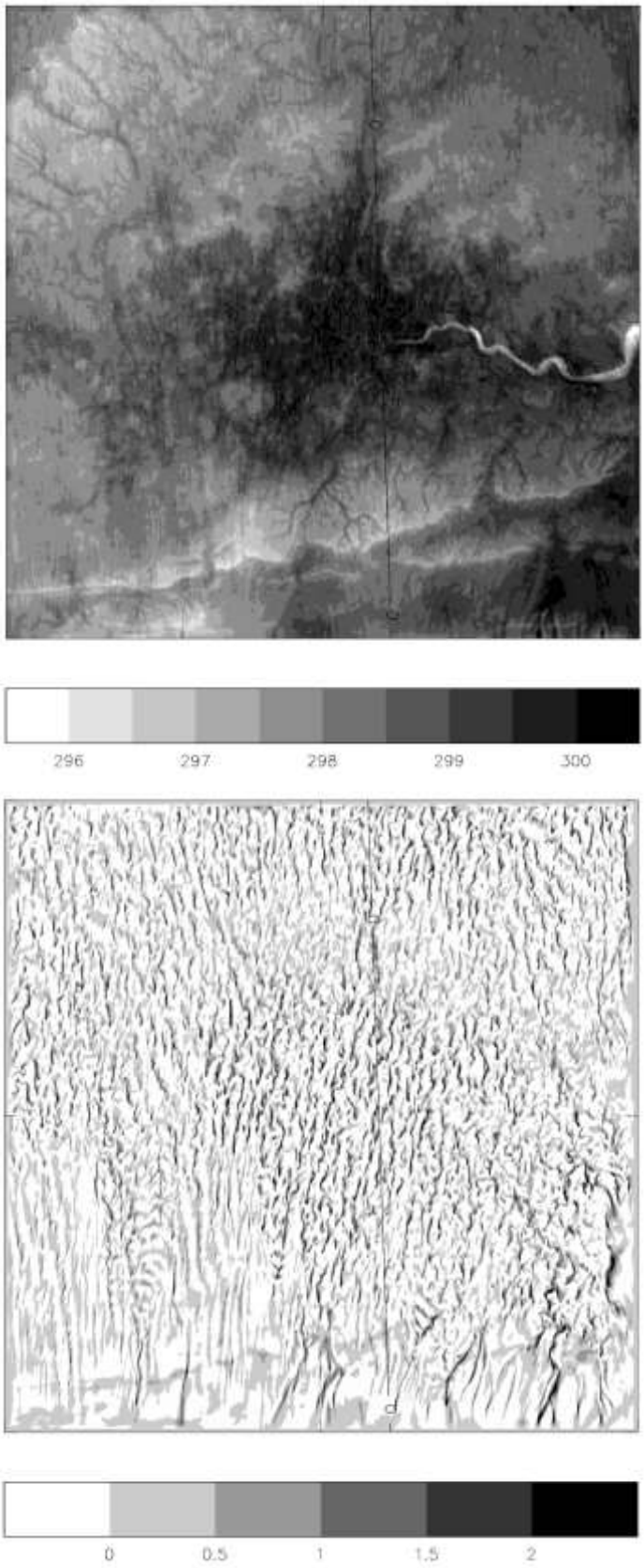

Figure 2 (a) 1.5m temperature field at 1400 UTC on the U100 domain. (b) Vertical velocity at 293m on the same domain.

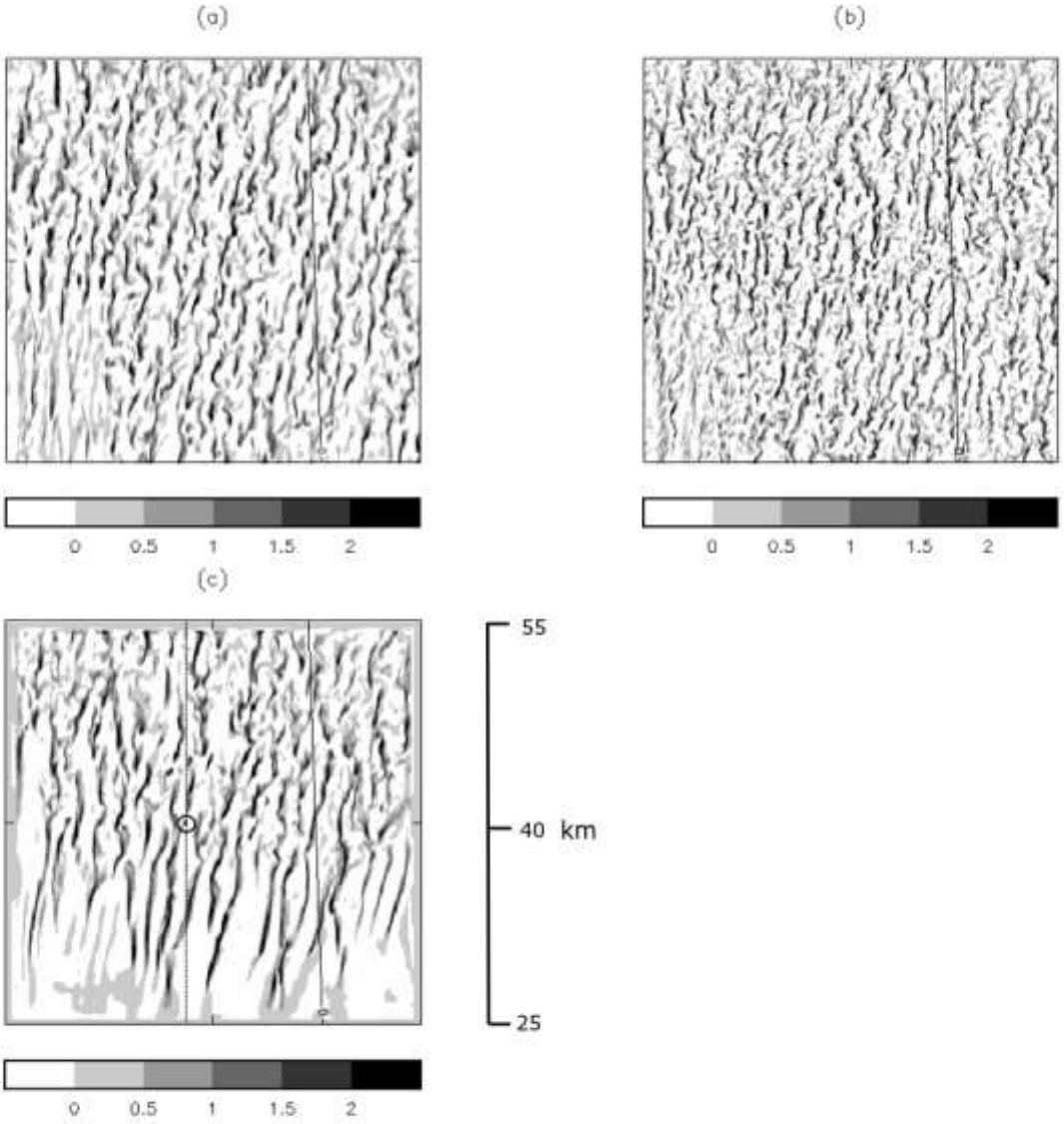

Figure 3. Vertical velocity at 293m in (a) U100, (b) U50 and (c) U100S. In all cases the area shown is that of the domain of U100S. The North-South dotted line in (c) represents the location of the transect used in Figures 10 and 11 and the centre of the circle on the transect is the location of the BT tower (WCC close by on this scale). The scale to the right of (c) represents locations in km on the transect comparable to those on Figures 10 and 11.

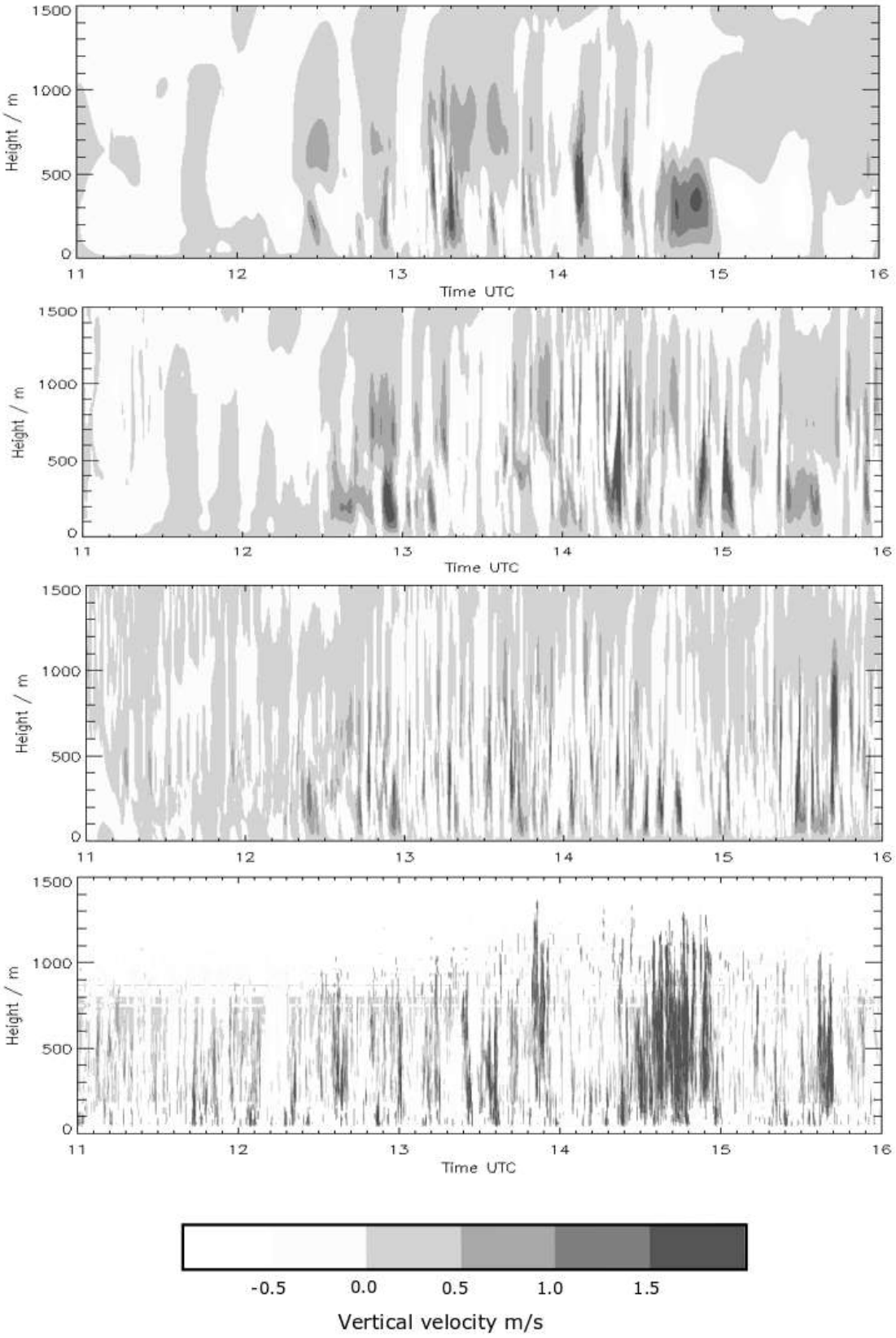

Figure 4. Time/height cross sections of vertical velocity at WCC in (a) U100S (b) U100, (c) U50 and (d) lidar observations.

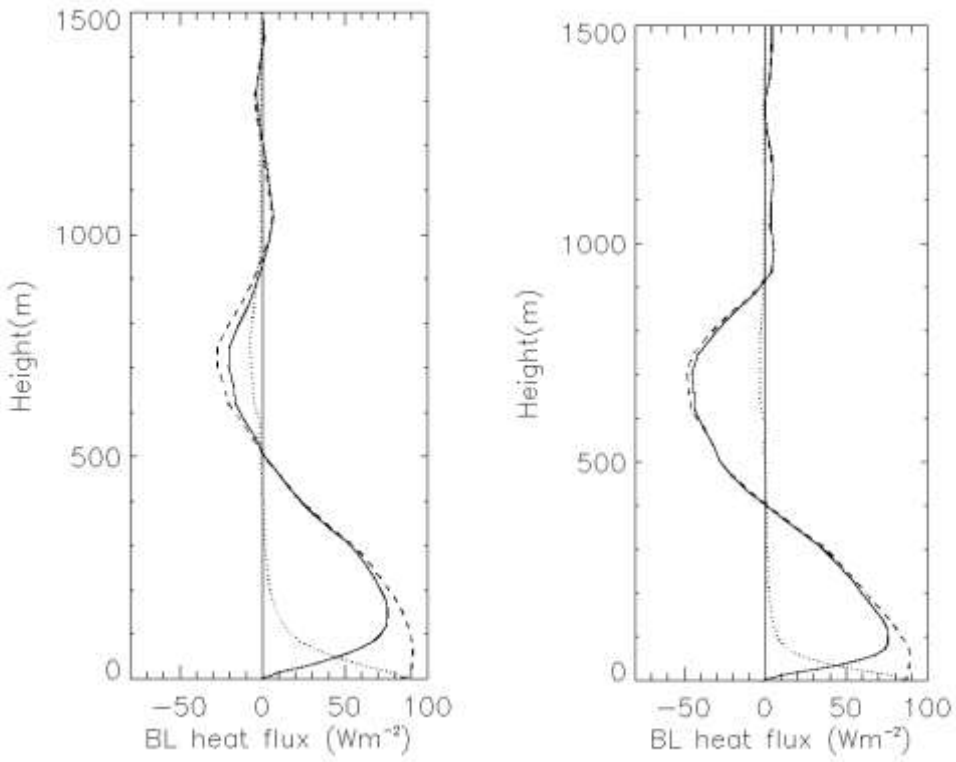

Figure 5. Profiles of sensible heat flux in U100 (left) U50. Dotted lines are parameterised flux, solid is explicit and dashed is total.

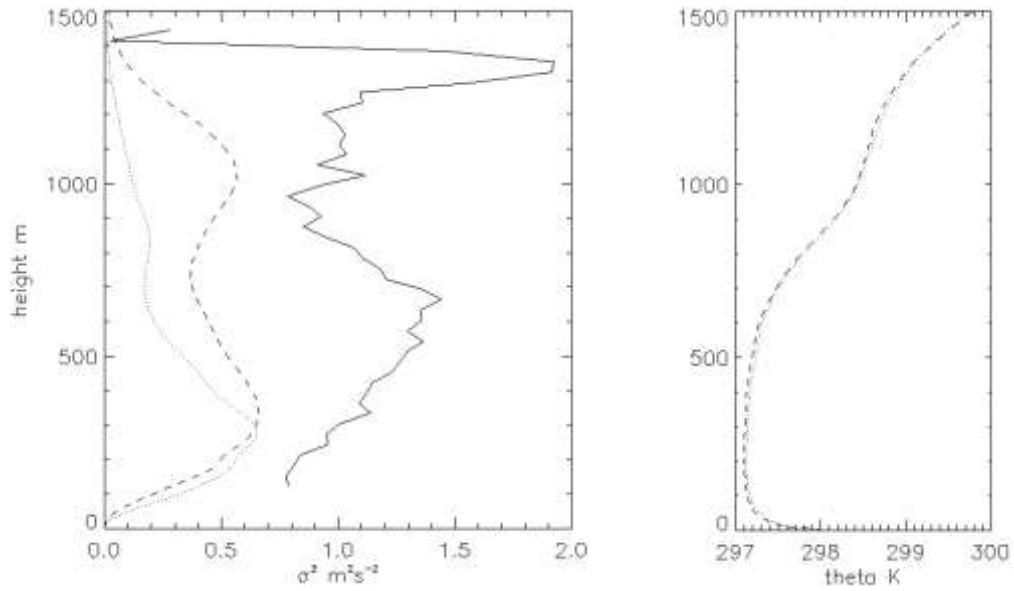

Figure 6. (a) Vertical velocity variance profiles from 1300-1400 UTC. Sold line is lidar data, dashed is U100 and dotted is U50 (b) theta profile in U100 and U50 averaged over a 2km box centred on the BT tower.

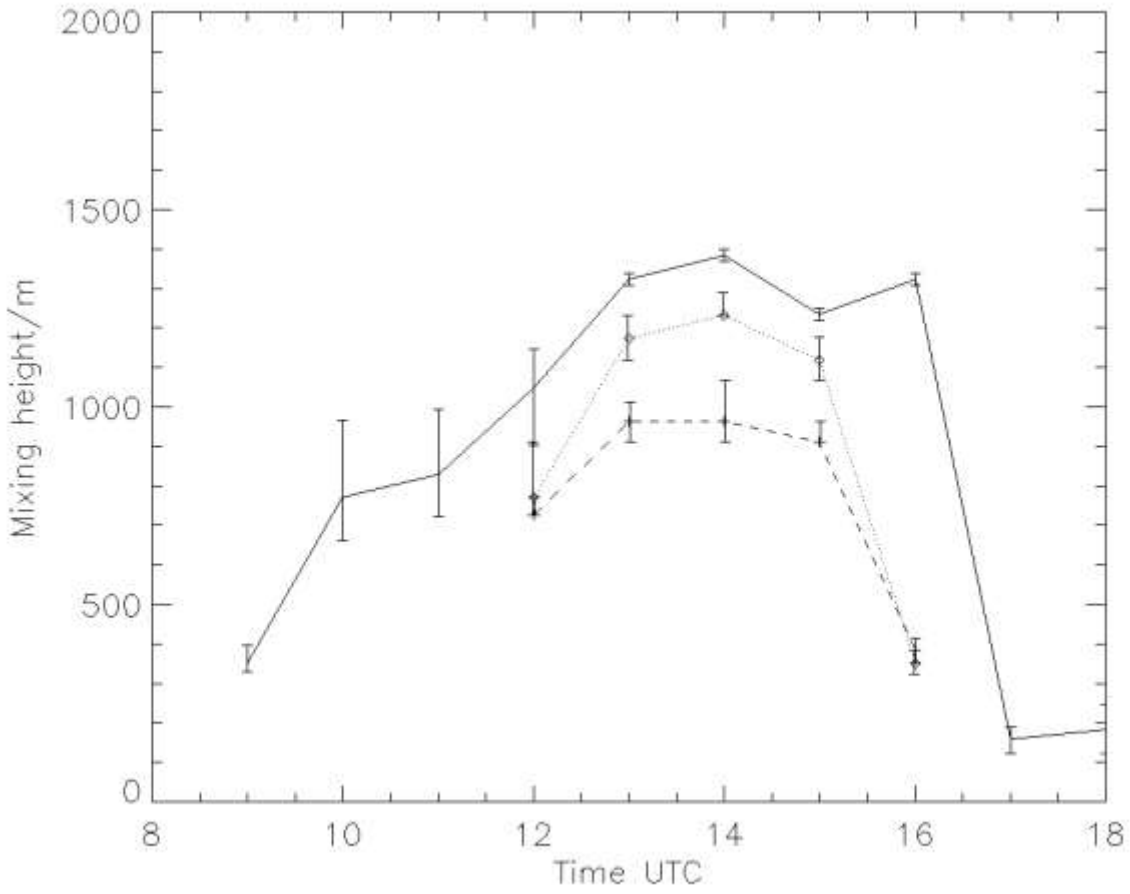

Figure 7. Mixing height at WCC as a function of time from lidar observations, U100 and U50. The mixing height was calculated using a variance threshold of 0.1 $m^2s\text{-}^2$.The solid line is lidar data, circles/dotted U100 and plus signs/dashes U50. Error bars were calculated by perturbing the variance threshold up and down by 30%.

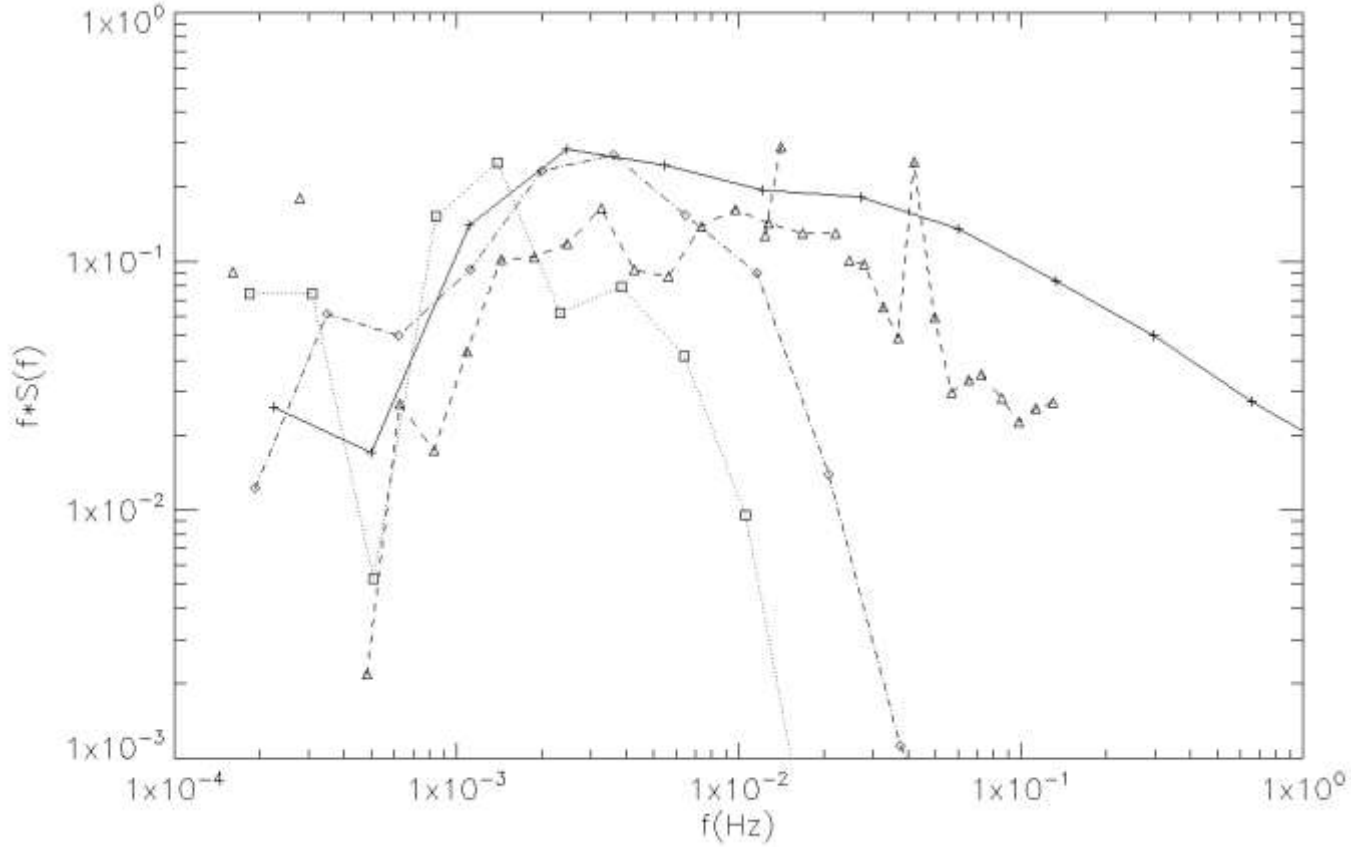

Figure 8. Spectra for U100 and U50 compared to lidar and BT tower observations for 1400 to 1600 UTC. Plus signs/sold lines BT tower, triangles/dashed lines lidar, diamonds/dash-dot U50 and squares/dotted lines U100.

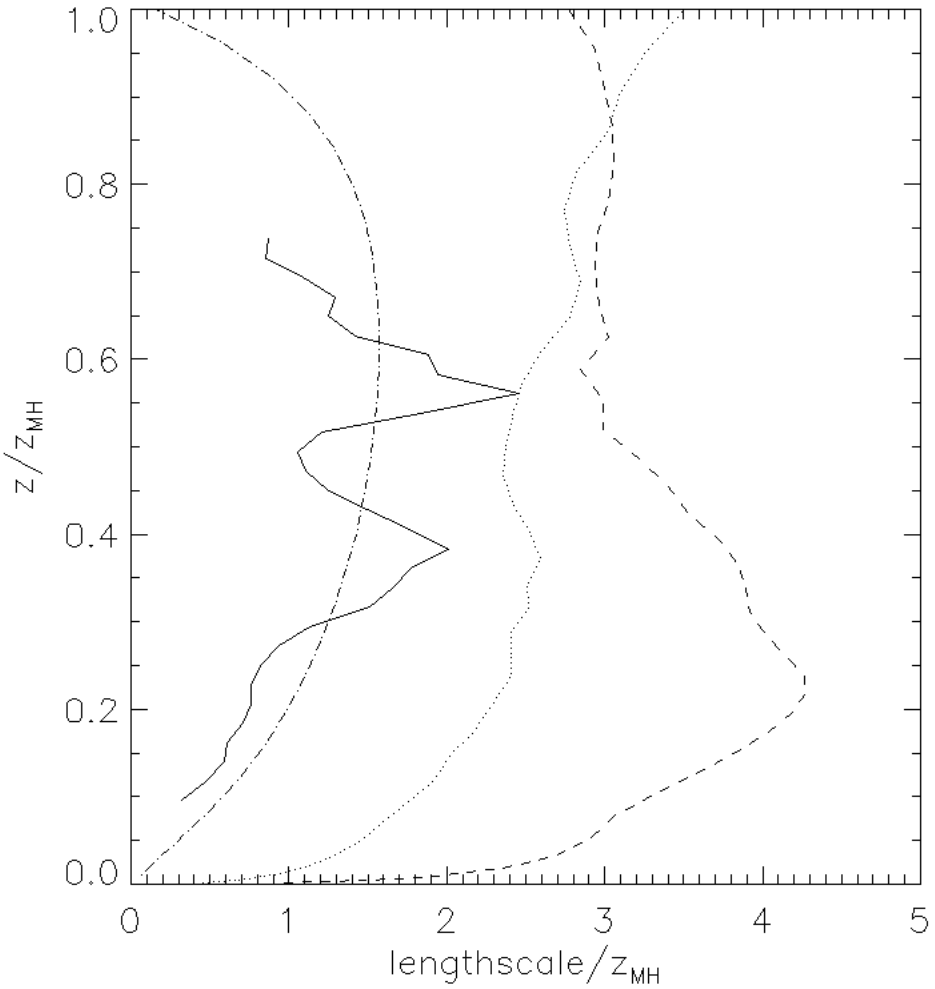

Figure 9. Turbulence lengthscale as a function of height for 1400 to 1600 UTC, normalised by mixing height. Solid line is lidar data, dotted line from U50, dashed line from U100 and dash-dot line from Caughey et al., 1979.

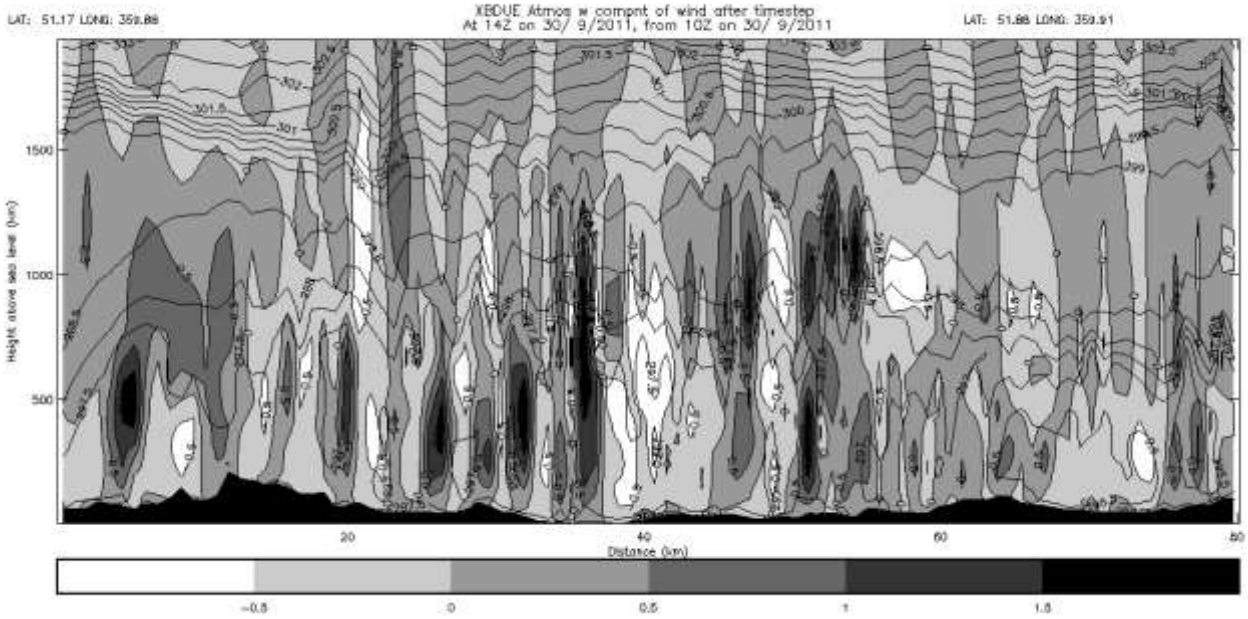

Figure 10. Cross section of vertical velocity field (shading) and potential temperature (theta) contours in U100 at 1400 UTC along south (left) to north transect through BT tower with orography also shown.

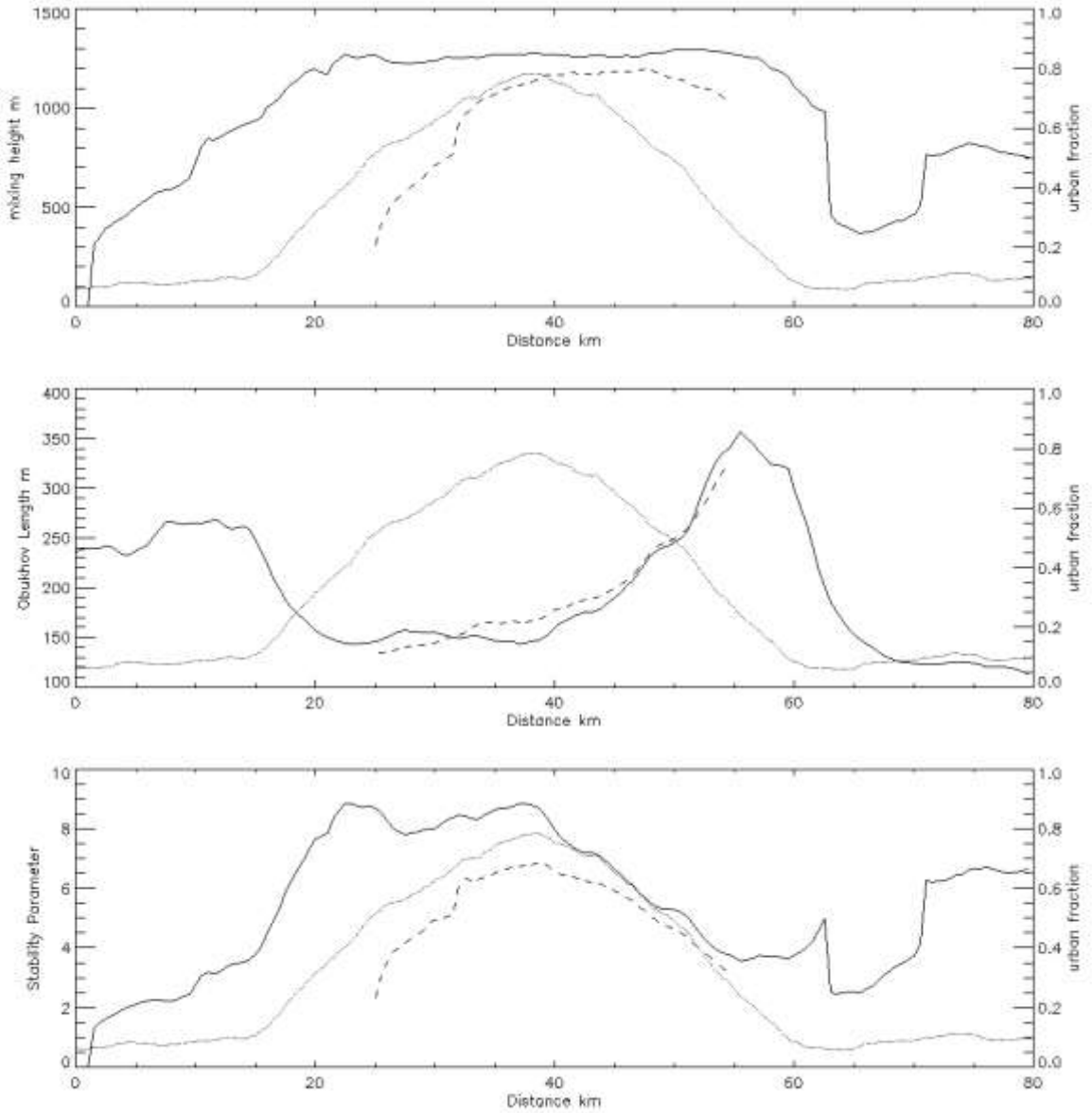

Figure 11. South to north transect through BT tower showing urban fraction (dotted line) and plots for U100 (solid line) and U100S (dashed line). (a) mixing heights, (b) obukhov length (absolute value), (c) stability parameter.

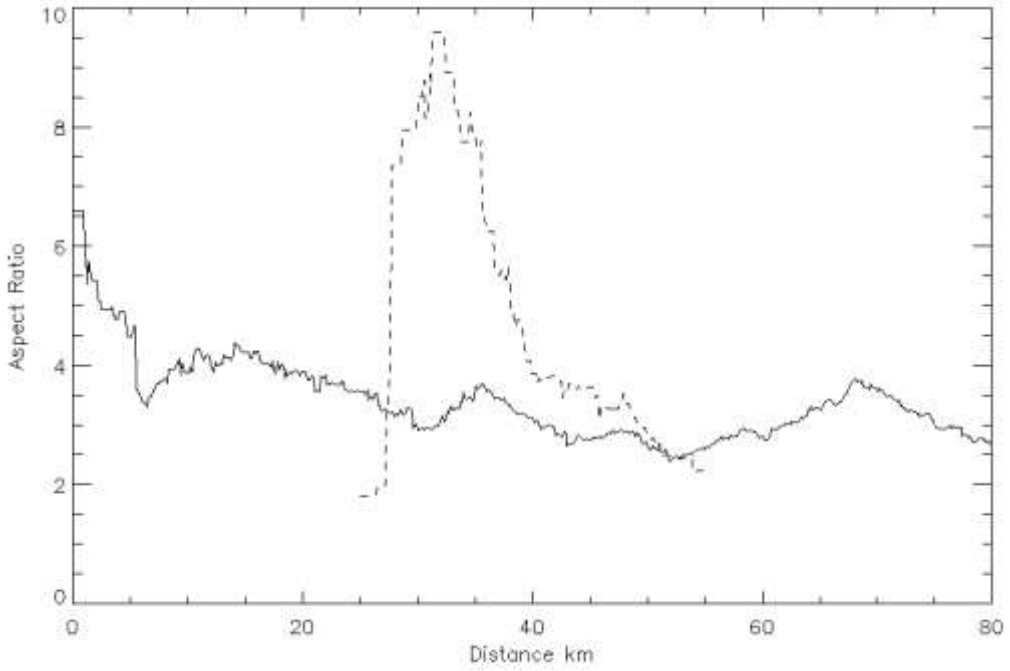

Figure 12. Aspect ratio of vertical velocity objects as a function of distance from the southern boundary of the domain for U100 and U100S (dashed line) 100m model. A vertical velocity threshold of 2.0 ms^{-1} was used on a vertical velocity field on model level 20 (290m above ground). The aspect ratio data was smoothed as a function of distance from the southern boundary using an averaging length of 3km.